Chapter 10
Strong Focusing Synchrotron

Abstract This Chapter introduces the strong focusing synchrotron, alternating gradient (AG) and separated focusing, and the theoretical material needed for the simulation exercises. It begins with a brief reminder of the historical context, and continues with beam optics, chromaticity, and acceleration. It relies on basic charged particle optics and acceleration concepts introduced in the previous Chapters, and further addresses the following aspects:
- resonances and resonant extraction,
- stochastic energy loss by synchrotron radiation.
The simulation of a strong focusing synchrotron requires just two, possibly three, optical elements from `zgoubi` library: DIPOLE, BEND, or MULTIPOL to simulate (possibly combined function) dipoles, DRIFT to simulate straight sections, and MULTIPOL to simulate lenses (which can be otherwise simulated using QUADRUPO, SEXTUPOL, OCTUPOLE, etc.). A fourth element, CAVITE, is required for acceleration. Particle monitoring requires keywords introduced in the previous Chapters, including FAISCEAU, FAISTORE, possibly PICKUPS, and some others. Spin motion computation and monitoring resort to SPNTRK, SPNPRT, FAISTORE. Optics matching and optimization use FIT[2]. INCLUDE is used, mostly here in order to shorten the input data files. SYSTEM is used to, mostly, resort to gnuplot so as to end simulations with some specific graphs obtained by reading data from output files such as zgoubi.fai (resulting from the use of FAISTORE), zgoubi.plt (resulting from IL=2), or other zgoubi.*.out files resulting from a PRINT command.

Notations used in the Text

B; $\mathbf{B}$, $B_{\mathrm{x,y,s}}$	field value; field vector, its components in the moving frame
$B\rho = p/q$; $B\rho_0$	particle rigidity; reference rigidity
C; C_0	orbit length, $C = 2\pi R + \left[\begin{smallmatrix}\text{straight}\\ \text{sections}\end{smallmatrix}\right.$; reference, $C_0 = C(p = p_0)$
E	particle energy
EFB	Effective Field Boundary
f_{rev}, $f_{\mathrm{rf}} = h\, f_{\mathrm{rev}}$	revolution and RF accelerating voltage frequencies
G	gyromagnetic anomaly, $G = 1.792847$ for proton
G; $K = G/B\rho$	quadrupole gradient; focusing strength
h	RF harmonic number
m; m_0; M	mass, $m = \gamma m_0$; rest mass; in units of MeV/c^2
$\mathbf{p}$; p; p_0	momentum vector; its modulus; reference
$P_i,\ P_f$	beam polarization, initial, final
q	particle charge
$r,\ R$	orbital radius ; average radius, $R = C/2\pi$
s	path variable
v	particle velocity
$V(t)$; $\hat{V}$	oscillating voltage; its peak value
x, x', y, y', l, $\frac{dp}{p}$	horizontal, vertical, longitudinal coordinates in moving frame
α	depending on the context: momentum compaction or trajectory deviation
$\beta = v/c$; β_0; β_{s}	normalized particle velocity; reference; synchronous
β_{u}	betatron functions ($u:\ x, y, Y, Z$)
$\gamma = E/m_0$	Lorentz relativistic factor
δp	momentum offset or Dirac distribution
Δp	momentum offset
ε	wedge angle
ε_{u}	Courant-Snyder invariant ($u:\ x, r, y, l, Y, Z, s$, etc.)
ϵ_R	strength of a depolarizing resonance
μ_{u}	betatron phase advance, $\mu_{\mathrm{u}} = \int_{\mathrm{period}} ds/\beta_{\mathrm{u}}(s)$ ($u:\ x, y, Y, Z$)
ν_{u}	wave numbers, horizontal, vertical, synchrotron ($u:\ x, y, Y, Z, l$)
$\rho,\ \rho_0$	curvature radius; reference
σ	beam matrix
ϕ; ϕ_{s}	particle phase at voltage gap; synchronous phase
ϕ_{u}	betatron phase advance, $\phi_{\mathrm{u}} = \int ds/\beta_{\mathrm{u}}$ ($u:\ x, y, Y, or Z$)
φ	spin angle to the vertical axis

10.1 Introduction

In the very manner that the 1930s-1940s cyclotron, betatron, microtron, weak focusing synchrotron, still in use today, have since essentially not changed in their

concepts, design principles, magnet gap profile, today's gap profile, yoke and current coil geometry of combined function alternating-gradient (AG) dipoles remain essentially as patented in 1950 (Fig. 10.1) [1].

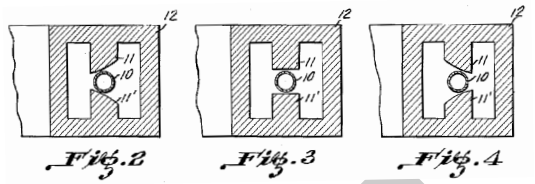

Fig. 10.1 Bending magnet pole profiles for a *focusing system for ions and electrons* [1]. Assuming curvature center to the left, the right (respectively left) profile is defocusing (resp. focusing), the middle profile has zero index

In 1952, in the context of studies relative to the Cosmotron, strong focusing was devised at the Brookhaven National Laboratory (BNL): *"Strong focusing forces result from the alternation of large positive and negative n-values in successive sectors of the magnetic guide field in a synchrotron. This sequence of alternately converging and diverging magnetic lenses* [...] *leads to significant reductions in oscillation amplitude"* [2]. It led to the construction of the first two high-energy proton AG synchrotrons, in the 30 GeV range, in the late 1950s: the proton-synchrotron (PS) at CERN, and the AGS at BNL, major pieces 60 years later still, of the respective injection chains of the two largest colliders in operation, the LHC and RHIC. Early works at BNL provided theoretical formalism, still at work today, for the analysis of beam dynamics in synchrotrons [3].

The optical principle behind the AG concept is that a doublet of focusing and defocusing lenses with proper strengths results in a short focal distance converging system. The dramatic reduction of transverse beam size by AG focusing allows small dipole gaps, thus small magnets: from lowest energies (medical synchrotrons in the 100 MeV range for instance) to the highest ones (particle physics and nuclear physics colliders, hundreds of GeV to multi-TeV range), beams are essentially confined in a centimeter scale transverse space, making a synchrotron a string of dipole magnets containing the beam in a ring vacuum pipe of a few centimeters in diameter (hadrons) or a few millimeters (electrons). The size of the ring is essentially determined by its circumference, proportional to the magnetic rigidity. This revolutionized the race to high energies, from the prior few GeV weak focusing synchrotrons and their huge magnets, to todays 7 TeV at the LHC with magnets transverse size of a few tens of centimeters, and with further plans for 100 TeV rings [5]. It fostered as well the development of high energy synchrotron light sources around the world, with electron beam energies up to 8 GeV.

Separated function focusing, whereby beam guiding is ensured by uniform field dipoles while focusing is ensured separately by quadrupoles, followed from the development of the latter (Fig.10.4), a spin-off of the strong index technology [9]. Separated function optics allows changing wave numbers at will (within the optical system stability limits). It allows introducing modular functions in complex rings such as dispersion suppression sections, low-beta or insertion device sections, long

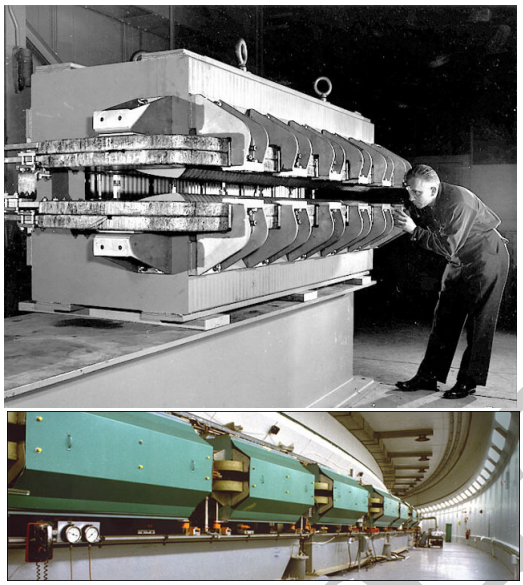

Fig. 10.2 Top: the AGS combined function main magnet - one of 240 steering the beam around the ring, bottom: the 809 m circumference AGS synchrotron [4]. The hyperbolic profile poles are visible on the top photo, partly hidden by the field coils

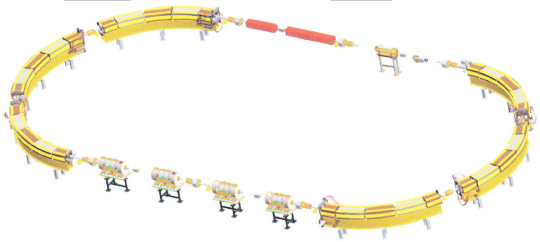

Fig. 10.3 The ion rapid cycling medical synchrotron (iRCMS) [6], an RCS aimed at providing ion beams for the treatment of cancer tumors

straights, etc. Low-emittance, high-brightness light source lattices have complicated focusing further, by introducing longitudinal field gradient bending systems, aimed at minimizing the chromatic invariant [10]. AG focusing however has the benefit of compactness and is still resorted to, today, in hadrontherapy applications (Fig. 10.3), light source lattice [7], and other high energy collider design [8].

Due to the necessary ramping of the field in order to maintain a constant orbit, synchrotron accelerators are pulsed, storage rings in some cases as well, high energy colliders in particular to bring beams to highest store energy. The acceleration is cycled and the accelerating voltage frequency as well in ion accelerators, from injection to top energy. If the ramping uses a constant electromotive force, then (Eq. 9.3)

$$B(t) \approx \frac{t}{\tau} \tag{10.1}$$

Fig. 10.4 A quadrupole magnet at LBL in 1957, used for beam lines at the 184-inch cyclotron. An early specimen here, obviously, being a spin-off of the early 1950s concept of strong focusing [11]

$\dot{B} = dB/dt$ does not exceed a few Tesla/second, thus the repetition rate of the acceleration cycle if of the order of a Hertz. If instead the magnet winding is part of a resonant circuit then the field oscillates,

$$B(t) = B_0 + \frac{\hat{B}}{2}(1 - \cos \omega t) \tag{10.2}$$

so that, in the interval of half a voltage repetition period (*i.e.*, $t : 0 \rightarrow \pi/\omega$) the field increases from an injection threshold value to a maximum value at highest rigidity, $B(t) : B_0 \rightarrow B_0 + \hat{B}$. The latter determines the highest achievable energy: $\hat{E} = pc/\beta = q\hat{B}\rho c/\beta$. The repetition rate with resonant magnet cycling can reach a few tens of Hertz, a technique known as a rapid-cycling synchrotron (RCS). In both cases anyway B imposes its law and the other parameters comprising the acceleration cycle the RF frequency in particular, will follow B(t).

Rapid cycling allows high intensity beams. Instances are the Cornell 12 GeV, 60 Hz, electron AG synchrotron, commissioned in 1967, still in use half a century later as the injector of Cornell 5 GeV synchrotron light source (CHESS); Fermilab 8 GeV, 60 Hz, booster which provides protons for the production of neutrino beams; the 30 GeV 500 kW beam J-PARC facility in Japan. Rapid cycling is also considered in ion-therapy applications, Fig. 10.3.

10.2 Basic Concepts and Formulæ

Alternating gradient focusing is sketched in Fig. 10.5.

The focusing index value can be estimated from the fields met in these structures: say a maximum B∼1 Tesla in the dipole gap, and as well at pole tip in quadrupoles ∼10 cm off axis. The latter results in $\frac{\Delta B}{\Delta x} \sim 10$ T/m, the former in meters to tens of meters dipole curvature radius. All in all,

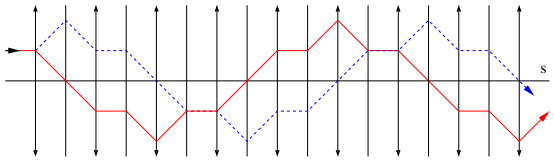

Fig. 10.5 Horizontally focusing lenses (field index $n \gg 0$, the solid red trajectory) are vertically defocusing ($n \ll 0$, the dashed blue trajectory), and vice versa. This imposes alternating gradients in order for a sequence to be globally focusing.

$$n = \frac{\rho}{B}\frac{\partial B}{\partial x} \sim \frac{10^{0\sim 2}_{[\mathrm{m}]}}{1_{[\mathrm{T}]}} \times 10_{[\mathrm{T/m}]} \sim 10^{1\sim 3} \quad \gg 1 \tag{10.3}$$

much greater than in a weak focusing structure, characterized by $0 < n < 1$.

10.2.1 Components of the Strong Focusing Optics

Combined function (AG) optics

This is, typically, the BNL AGS and CERN PS optics, using dipoles that ensure both beam guiding and focusing (Fig. 10.2). Separate quadrupole and multipole lenses have later been introduced in these lattices as they provide knobs for the adjustment of optical functions and parameters.

AG optics is still at work in modern designs, as in the iRCMS whose six 60 deg arcs are comprised of a sequence of five focusing and defocusing combined function dipoles [6], Fig. 10.3.

Field

Referring to the normal conducting magnet technology, an hyperbolic pole profile (Fig. 10.1) is an equipotential of equation

$$V(x, y) = A\, x\, y$$

This pole profile therefore results in

$$B_y = \frac{\partial V}{\partial y} = A\, x, \quad \textit{i.e.}\ \text{a radial field index} \quad n = \frac{\rho}{B_y}\frac{\partial B_y}{\partial x}|_{\mathrm{y=0}} = \frac{\rho}{B_y} A$$

responsible for the focusing. A is a constant, typically ~ 10 T/m in normal conducting magnets, *cf.* Eq. 10.3. (an order of magnitude greater with SC technology). The pole profile opens up either inward (toward the center of curvature, a horizontally focusing

dipole, vertically defocusing) or outward (a vertically focusing dipole, horizontally defocusing), Fig. 10.6.

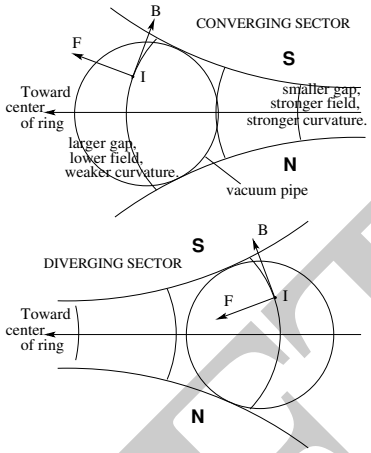

Fig. 10.6 Beam focusing in combined function dipoles. The center of curvature is to the left. The pole profile follows an equipotential $V = Axy$. Top: the pole profile opens up towards the center of curvature → the dipole is horizontally converging (vertically diverging: current I comes out of the page, force **F** results from field **B**). Bottom: pole profile closing toward the center of curvature → the dipole is horizontally diverging, vertically converging

In a bent AG dipole a line of constant field is an arc of a circle; the field guides the reference particle along the arc in the median plane. The mid-plane field can be expressed as

$$B_y(r,\theta) = \mathcal{G}(r,\theta)\, B_0 \left(1 + n\,\frac{r-r_0}{r_0} + n_2 \left(\frac{r-r_0}{r_0}\right)^2 + n_3 \left(\frac{r-r_0}{r_0}\right)^3 + \ldots\right) \quad (10.4)$$

with r_0 the reference radius. Higher order indices, sextupole n_2, octupole n_3, ..., may be residual effects: fabrication tolerance, saturation, magnetic permeability, deformation of yoke with years, ..., as in the AGS dipoles, or included by design.

In a straight AG dipole a line of constant field is a straight line; an instance is the AGS main magnet (Fig. 10.2). Another instance is the Fermilab recycler arcs permanent magnet dipole, which includes quadrupole and sextupole components [12, 13]. The modeling of the field in a straight combined function dipole can be derived from the scalar potential of Eq. 10.5.

Separated function optics

In a separated funcion lattice main bends have zero index and ensure beam guiding, quadrupole lenses, alternately focusing and defocusing, ensure the essential of the focusing. In smaller rings though, bending contributes horizontal focusing (see Sect. 9.2.1.2, Fig. 9.6), wedge angles in addition may be introduced and contribute some horizontal and vertical focusing/defocusing (Fig. 9.9).

Higher order multipole lenses are used for the compensation of adverse effects: coupling, aberrations, space charge, impedance, etc., and for beam manipulations: coupling, resonant extraction, etc.

The field in a multipole of order n (n = 1, 2, 3, ...: dipole, quadrupole, sextupole, ...) derives, via $\mathbf{B} = \mathbf{grad}V$, from the Laplace potential [15]

$$V_n = (n!)^2 \left\{ \sum_{q=0}^{\infty} (-)^q \alpha_{n,0}^{(2q)}(s) \frac{(x^2+y^2)^q}{4^q q!(n+q)!} \right\} \left\{ \frac{x^{n-m}y^m}{m!(n-m)!} \sin m\frac{\pi}{2} \right\} \tag{10.5}$$

wherein $\alpha_{n,0}^{(2q)} = d^{2q}\alpha_{n,0}/ds^{2q}$ accounts for the s-dependence of the field. Technologies for multipoles and combined multipoles include pole profiling, permanent magnets [12, 17], superconducting $\cos\theta$ windings as in RHIC and LHC colliders, and variants of all sorts.

In a hard-edge model the left sum in Eq. 10.5 is reduce to the $q = 0$ term, with the following outcomes.

Quadrupole

The equipotential (the pole profile) is an hyperbola: Gxy =constant, in an upright quadrupole (left), and $G(x^2 - y^2)$ =constant in a $\pi/4$ skewed quadrupole (right); the resulting field writes

$$B_x = \frac{\partial V}{\partial x} = Gy \qquad B_y = \frac{\partial V}{\partial y} = Gx$$

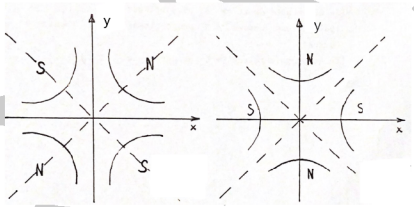

$$B_x = Gx \qquad B_y = -Gy$$

Upright quadrupoles are used for focusing, skew quadrupoles are used to compensate, or introduce, transverse coupling. Their focusing strength

$$K = \frac{1}{L}\frac{\int G(s)\,ds}{p/q}$$

is momentum-dependent.

Sextupole

The equipotential satisfies $H(3x^2y - y^3)$ =constant in an upright sextupole (left), $H(x^3 - 3xy^2)$ =constant in a $\pi/6$ skewed sextupole (right), with resulting field

$B_x = 2Hxy$
$B_y = H(x^2 - y^2)$

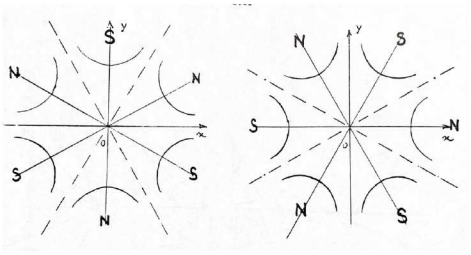

$B_x = H(x^2 - y^2)$
$B_y = -2Hxy$

Upright sextupoles introduce a vertical field component $B_y \propto x^2$, they are used to correct optical aberrations, to modify the momentum dependence of the wave numbers ν_x, ν_y, and in beam manipulations such as resonant extraction. Skew sextupoles introduce a radial field component $B_x \propto y^2$, they are used to correct optical aberrations.

Octupole

The equipotential pole profile satisfies $O(x^3y - xy^3)$ =constant in an upright octupole (left), $O(x^4 - 6x^2y^2 + y^4)$ =constant in a $\pi/8$ skewed octupole (right), yielding the field

$B_x = O(3x^2y - y^3)$
$B_y = O(x^3 - 3xy^2)$

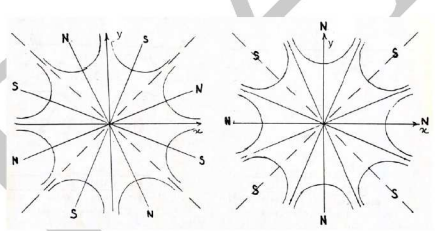

$B_x = O(x^3 - 3xy^2)$
$B_y = -O(3x^2y - y^3)$

Upright octupoles are used to introduce a vertical field component $B_y \propto x^3$; skew octupoles introduce a vertical field component $B_y \propto y^3$. Octupoles are used to correct aberrations, or to modify the amplitude dependence of wave numbers.

10.2.2 Transverse motion

The transverse motion of a particle in the periodic lattice of a cycic accelerator satisfies Hill's equations

$$\frac{d^2x}{ds^2} + K_x(s)x = \frac{1}{\rho_0}\frac{\Delta p}{p_0}, \qquad \frac{d^2y}{ds^2} + K_y(s)y = 0 \tag{10.6}$$

where $K_x(s)$, $K_y(s)$ have the periodicity of the lattice, and depend locally on the nature of the optical elements:

$$\begin{aligned}
&\text{– dipole :} && \begin{cases} K_x = \dfrac{1-n}{\rho_0^2} \\ K_y = \dfrac{n}{\rho_0^2} \end{cases} \qquad (n = -\tfrac{\rho_0}{B_0}\tfrac{\partial B_y}{\partial x}) \\
&\text{– a wedge at } \mathrm{s = s_w} : && \left\{ K_{\substack{x \\ y}} = \pm\frac{\tan\varepsilon}{\rho_0}\delta(s - s_w) \right. \quad \left(\text{with } \varepsilon \lessgtr 0 \text{ for } \begin{matrix}\text{focusing} \\ \text{defocusing}\end{matrix} \right) \\
&\text{– quadrupole} && (\text{gradient } G = \tfrac{\text{field at pole tip}}{\text{radius at pole tip}}) : K_{\substack{x \\ y}} = \frac{\pm \mathrm{G}}{B\rho};\ \frac{1}{\rho_0} = 0 \\
&\text{– drift space :} && K_x = K_y = 0;\ \frac{1}{\rho_0} = 0
\end{aligned} \tag{10.7}$$

By contrast with the betatron and weak focusing technologies, strong focusing with its independent focusing ($G > 0$) and defocusing ($G < 0$) families allows separate adjustment of the horizontal and vertical focusing strengths, and wave numbers as a consequence.

The on-momentum ($p = p_0$) closed orbit coincides with the reference axis of the optical structure. The betatron motion for an on-momentum particle satisfies Eq. 10.6 with $\Delta p = 0$. Solving the latter (see Sect. 9.2) requires introducing two independent solutions $u_{\substack{1 \\ 2}}(s)$ (Eq. 9.12), the linear combination of which yields the pseudo harmonic motion (Eq. 9.15)

$$\begin{cases} u(s) = \sqrt{\beta(s)\varepsilon/\pi}\,\cos\left(\int \dfrac{ds}{\beta(s)} + \varphi\right) \\ u'(s) = -\sqrt{\dfrac{\varepsilon/\pi}{\beta(s)}}\,\sin\left(\int \dfrac{ds}{\beta(s)} + \varphi\right) + \alpha(s)\,\cos\left(\int \dfrac{ds}{\beta(s)} + \varphi\right) \end{cases} \tag{10.8}$$

The motion satisfies the Courant-Snyder invariant, namely (Fig. 9.10)

$$\gamma_u(s)u^2 + 2\alpha_u(s)uu' + \beta_u(s)u'^2 = \frac{\varepsilon_u}{\pi} \tag{10.9}$$

The form and the orientation of this phase space ellipse change along the period, more than in a weak focusing lattice as a consequence of the strong modulation of the betatron functions (Fig. 10.7), a consequence of the strong focusing. The surface of the ellipse does not change.

Beam envelopes are given by the extrema,

$$\hat{x}_{\mathrm{env}}(s) = \pm\sqrt{\beta_x(s)\frac{\varepsilon_x}{\pi}}, \qquad \hat{y}_{\mathrm{env}}(s) = \pm\sqrt{\beta_y(s)\frac{\varepsilon_y}{\pi}} \tag{10.10}$$

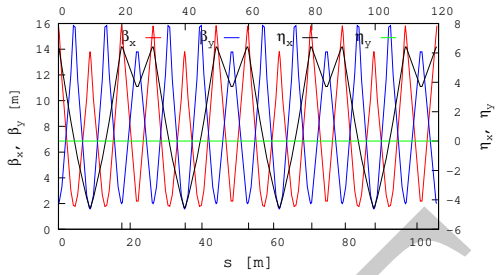

Fig. 10.7 Optical functions in SATURNE II synchrotron (see exercise 10.1)

Phase space motion

Write the two independent solutions $u_{\frac{1}{2}}(s)$ (Eq. 9.12) under the form

$$u_1(s) = \underbrace{F(s)}_{\text{S-periodic}} \times \underbrace{e^{i\mu\frac{s}{S}}}_{\frac{2\pi S}{\mu}\text{-periodic}} \quad \text{and} \quad u_2(s) = u_1^*(s) = F^*(s)\, e^{-i\mu\frac{s}{S}} \tag{10.11}$$

wherein $F(s) = \sqrt{\beta(s)}\, e^{\,i\left(\int_0^s \frac{ds}{\beta(s)} - \mu\frac{s}{S}\right)}$. Introduce $\psi(s) = \int_0^s \frac{ds}{\beta(s)} - \mu\frac{s}{S}$ so that $F(s) = \sqrt{\beta(s)}\, e^{i\psi(s)}$, Eq. 10.8 thus takes the form

$$\left|\begin{array}{l} u(s) = \overbrace{\sqrt{\beta(s)\varepsilon/\pi}}^{S\text{-periodic}}\ \overbrace{\cos\left[\nu\frac{s}{R} + \underbrace{\psi(s)}_{\text{S-per.}} + \varphi\right]}^{\frac{2\pi S}{\mu}\text{-periodic}} \\ u'(s) = -\sqrt{\frac{\varepsilon/\pi}{\beta(s)}}\ \sin\left[\nu\frac{s}{R} + \psi(s) + \varphi\right] + \alpha(s)\ \cos\left[\nu\frac{s}{R} + \psi(s) + \varphi\right] \end{array}\right. \tag{10.12}$$

wherein $\nu = \dfrac{N\mu}{2\pi}$. Thus, as th betatron function $\beta(s)$ and phase $\psi(s)$ are S-periodic, the turn-by-turn motion observed at a given azimuth s (*i.e.*, $u(s)$, $u(s+\mathcal{S})$, $u(s+2\mathcal{S})$, ...) is sinusoidal and its frequency is $\nu = N\mu/2\pi$. Successive particle positions $(u(s), u'(s))$ in phase space lie on the Courant-Snyder invariant (Eq. 10.9).

The wave numbers ν_x and ν_y can be adjusted independently in a separated function lattice, by means of two independent quadrupole families. The working point (ν_x, ν_y) fully characterizes the first order optical setting of the ring.

Off-momentum motion

The motion of an off-momentum particle satisfies the inhomogeneous Hill's horizontal differential Eq. 10.6. The chromatic closed orbit

$$x_{\mathrm{ch}}(s) = D_x(s)\frac{\delta p}{p} \tag{10.13}$$

is a particular solution of the equation, its periodicity is that of the cell.

By contrast with the weak focusing configuration, where the on-momentum closed orbit and chromatic closed orbits are parallel (Eq. 9.26: D_x=constant, independent of s), chromatic closed orbits in a strong focusing optical structure are distorted (Fig. 10.7), their excursion depends on the distribution along the cell of (i) the dispersive elements which are the dipoles, and (ii) the focusing.

The horizontal motion of an off-momentum particle is a superposition of the particular solution (Eq. 10.13) and of the betatron motion, solution of the homogeneous Hill's equation (Eq. 10.6 with $\delta p/p = 0$), namely

$$x(s) = x_\beta(s) + x_{\mathrm{ch}}(s) = \sqrt{\beta_x(s)\frac{\varepsilon_x}{\pi}}\,\cos\left(\int\frac{ds}{\beta_x} + \varphi\right) + D_x(s)\frac{\Delta p}{p_0} \tag{10.14}$$

whereas the vertical motion is unchanged (Eq. 10.12 taken for $u(s) \equiv y(s)$).

10.2.3 Resonances

Consider the excitation of transverse beam motion by a generator of frequency Ω located at some azimuth along the ring [18]. The action of the excitation $S \times \sin\Omega t$ on the oscillating motion $u(t)$ can be written under the form

$$\frac{d^2u}{dt^2} + \omega^2 u = S\sin\Omega t \tag{10.15}$$

Assume harmonic motion for simplicity (as in a weak focusing lattice). Take S constant, the solution (superposition of the solution of the homogeneous differential equation and of a particular solution of the inhomogeneous differential equation) writes

$$u(t) = U\cos(\omega t + \varphi) + \frac{S}{\omega^2 - \Omega^2}\sin\Omega t \tag{10.16}$$

If betatron motion and excitation are in synchronism, *i.e.* on the resonance, $\omega = \Omega$, a particular solution of Eq. 10.15 is

$$u_r(t) = -\frac{S\,t}{2\Omega}\cos\Omega t$$

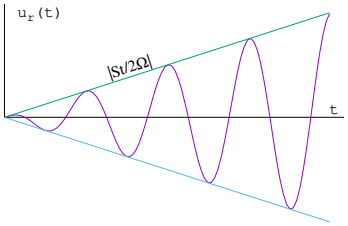

the amplitude of the oscillatory motion grows rapidly with time, at a rate $|St/2\Omega|$.

Assume S periodic instead, take its Fourier expansion $S(t) = \sum_{p=0}^{\infty} a_p \cos(p\omega' t + \varphi_p)$, the equation of motion thus writes

$$\frac{d^2u}{dt^2} + \omega^2 u = \sum_{p=0}^{\infty} a_p \cos(p\omega' t + \varphi_p)\ \sin\Omega t =$$

$$\sum_{p=0}^{\infty} \frac{a_p}{2}\Big[\sin[(\Omega - p\omega')t + \varphi_p] + \sin[(\Omega + p\omega')t + \varphi_p]\Big]$$

Resonance may occur at oscillator frequencies $\omega = \Omega \pm p\omega'$, their strength depends on the amplitude a_p of the excitation harmonics. If the generator is located at one point in the ring, it excites all harmonics.

Sextupole and octupole resonances

The horizontal motion in the presence of a sextupole component $(B_y(\theta)|_{y=0} = S(\theta)x^2$, see *Sextupole*, above) as part of the ring optical lattice satisfies

$$\frac{d^2x}{d\theta^2} + \nu_x^2 x = S(\theta)x^2 \tag{10.17}$$

Assume weak perturbation of the motion, so that $x(\theta) \approx \hat{x}\cos(\nu_x\theta + \varphi)$, the solution for unperturbed motion, and $S(\theta)$ 2π-periodic. Substitute its Fourier series expansion $S(\theta) = \sum_{p=0}^{\infty} a_p \cos(p\omega'\theta + \varphi_p)$ in Eq. 10.17, develop to get

$$\frac{d^2x}{d\theta^2} + \nu_x^2 x = \frac{\hat{x}^2}{2}\sum_{p=0}^{\infty} a_p\Big[\cos(p\theta + \varphi_p) +$$

$$\cos[(p - 2\nu_x)\theta + \varphi_p - 2\varphi]\ +\ \cos[(p + 2\nu_x)\theta + \varphi_p + 2\varphi]\Big]$$

Thus resonance may occur at betatron frequency families $\nu_x = \pm p$, $\nu_x = \pm(p - 2\nu_x)$, and $\nu_x = \pm(p + 2\nu_x)$, *i.e.*,

$$\begin{bmatrix} \nu_x = \text{integer} \\ 3\nu_x = \text{integer} \end{bmatrix}$$

In the case of a single sextupole in the ring, all the harmonics p are excited with the same amplitude a_p.

An octupole perturbation introduces a field component $B_y(\theta)|_{y=0} = O(\theta)x^3$ (see *Octupole*, above) in the optical lattice. In a similar way, assume weak perturbation so that $x(\theta) \approx \hat{x}\cos(\nu_x\theta + \varphi)$, and to $O(\theta)$ substitute its Fourier expansion. This yields the resonant betatron frequencies

$$\begin{bmatrix} \nu_x = \text{integer} \\ 2\nu_x = \text{integer} \\ 4\nu_x = \text{integer} \end{bmatrix}$$

Resonances in a general manner occur at betatron frequencies satisfying

$$m\nu_x + n\nu_y = \text{integer}$$

with the property that

$$\frac{\varepsilon_x}{m} - \frac{\varepsilon_y}{n} = \text{constant}, \qquad \text{an invariant of the motion}$$

with the following consequences:

- if m and n have opposite signs the resonance causes energy exchange between the horizontal and vertical motions: $\frac{\varepsilon_x}{|m|} + \frac{\varepsilon_y}{|n|} = \text{constant}$, an increase of ε_x correlates with a decrease of ε_y and vice-versa; in the presence of linear coupling for instance, $\nu_x - \nu_y = \text{integer}$, $\varepsilon_x + \varepsilon_y = \text{constant}$. An increase in motion amplitude anyway may cause particle loss, an issue in cyclotrons for instance where the Walkinshaw resonance $\nu_x = 2\nu_y$ causes vertical beam loss due to the increase of ε_y;
- if m and n have the same sign the resonance induces motion instability: $\frac{\varepsilon_x}{m} - \frac{\varepsilon_y}{n} = \text{constant}$, ε_x and ε_y may both increase with no limit.

10.2.4 Synchrotron Motion

Particle motion in the longitudinal phase space (phase, momentum) is determined by the lattice and by the acceleration parameters. The synchrotron acceleration technique has been discussed in Sect. 9.2.2: acceleration parameters include RF voltage $\hat{V}$, frequency $f_{rf} = \omega_{rf}/2\pi = hf_{rev}$, the synchronous phase ϕ_s. The synchrotron angular frequency is

$$\Omega_s = (\omega_{rev}^2\,|\eta| h_{RF} e\hat{V}\cos\phi_s \;/\; 2\pi E_s)^{1/2}$$

with $\eta = 1/\gamma^2 - \alpha$ the phase slip factor (Eq. 9.33) and $\alpha = 1/\gamma_{tr}^2 = \dfrac{\Delta C}{C}\Big/\dfrac{\Delta p}{p_0}$ the momentum compaction. The transition gamma γ_{tr} is a property of the lattice and determines the proper synchronous phase region for acceleration, either $[0, \pi/2]$ or $[\pi/2, \pi]$ (Fig. 9.15).

The bucket height, "momentum acceptance", satisfies

$$\pm\frac{\Delta p}{p} = \pm\frac{1}{\beta}\sqrt{\frac{q\hat{V}}{\pi h\eta E_s}\left[-(\pi - 2\varphi_s)\sin\varphi_s + 2\cos\varphi_s\right]} \tag{10.18}$$

The maximum extent in phase for small amplitude oscillations satisfies

$$\pm\Delta\varphi_{\max} = \frac{h\eta E_s}{p_s R_s \Omega_s} \times max\left(\frac{\Delta E}{E_s}\right) \tag{10.19}$$

****** separatrix **********

The motion of a particle with energy offset $\delta E = E - E_s$ satisfies the longitudinal invariants

$$\epsilon_l = \frac{\alpha E_s}{2\Omega_s}\left[\left(\frac{\delta E}{E_s}\right)^2 + \frac{1}{\Omega_s^2}\left(\frac{d}{dt}\frac{\delta E}{E_s}\right)^2\right] \tag{10.20}$$

$$(\widehat{\delta E})^2 = (\delta E)^2 + \frac{1}{\Omega_s^2}\left(\frac{d\delta E}{dt}\right)^2 \tag{10.21}$$

Introducing the squared *rms* relative synchrotron amplitude $\sigma^2_{\widehat{\delta E}/E} \equiv (\widehat{\delta E}/E_s)^2$ this yields in addition

$$\epsilon_l = \frac{\alpha E_s}{2\,\Omega_s}\,\sigma^2_{\widehat{\delta E}/E} \tag{10.22}$$

10.2.5 Radiative Energy Loss

A particle of rest mass m_0 and charge e traveling in a magnetic field is subject to stochastic photon emission, which causes energy loss [21]. The phenomenon involves two random processes:

- the probability of photon emission over a trajectory arc δs, a Poisson law,

$$p(k) = \frac{\Lambda^k}{k!}e^{-\Lambda} \qquad \text{with} \quad \Lambda =< k >=< k^2 > \tag{10.23}$$

wherein k is the number of photons emitted over δs, $\Lambda = \frac{5er_0}{2\hbar\sqrt{3}}B\rho\frac{\delta s}{\rho}$ is its average value, $r_0 = e^2/\,4\pi\epsilon_0 m_0 c^2$ is the classical radius of the particle, $\epsilon_0 = 1\,/\,36\pi 10^9$, $\hbar$ is the Plank constant,

- the energy ϵ of the photon(s), following the probability law

$$\mathcal{P}\left(\frac{\epsilon}{\epsilon_c}\right) = \frac{3}{5\pi}\int_0^{\epsilon/\epsilon_c}\frac{d\epsilon}{\epsilon_c}\int_{\epsilon/\epsilon_c}^{\infty} K_{5/3}(x)dx \tag{10.24}$$

with $K_{5/3}$ the modified Bessel function, $\gamma = E/E_0$ with $E_0 = m_0c^2$ the rest energy, and ϵ_c the critical energy of the radiation,

$$\epsilon_c = \frac{3\hbar\gamma^3 c}{2\rho} \tag{10.25}$$

The average energy loss over δs is, assuming ultra-relativistic particles: $\beta = v/c \approx 1$,

$$\delta E = \frac{2}{3} r_0 E_0 \gamma^4 \frac{\delta s}{\rho^2} = \frac{2}{3} r_0 e c \gamma^3 B \frac{\delta s}{\rho} \quad \underbrace{\approx 1.88\ 10^{-15}\ \gamma^3 \frac{\delta s}{\rho^2}}_{\text{for electrons}} \tag{10.26}$$

The energy spread resulting from the stochastic emission is

$$\sigma_{\delta E/E} = \frac{\sqrt{110\sqrt{3}\hbar c\ /\ \pi\epsilon_0}}{24 E_0/e}\ \gamma^{5/2}\ \frac{\sqrt{\delta s}}{\rho^{3/2}} \quad \underbrace{\approx 3.80\ 10^{-14}\ \gamma^{5/2} \frac{\sqrt{\delta s}}{\rho}}_{\text{for electrons}} \tag{10.27}$$

In a storage ring the RF system restores on average the energy lost by SR. Useful formulas are given in Tab. 10.1, in particular, assuming a flat ring the partition of energy between radial and longitudinal motions is determined by the partition numbers

$$\mathrm{J_x} = 1 - \mathcal{D},\ \ \mathrm{J_y} = 1,\ \ \mathrm{J_l} = 2 + \mathcal{D},\ \ \text{with } \mathcal{D} = \frac{\overline{\mathrm{D_x}(1-2\mathrm{n})/\rho^3}}{\overline{\rho^2}} \tag{10.28}$$

where $\overline{(*)}$ denotes an average over the ring circumference.

Damping of accelerated motion

In an accelerator (a light source injector for instance), the RF voltage increases during acceleration in order to compensate the increasing energy loss. To first order in the invariant ε_u (with u standing for x or y) transverse damping in the presence of acceleration satisfies [16]

$$\frac{d\varepsilon_u}{dt} = -\frac{2}{\tau_u(t)}\varepsilon_u + C_u(t) - \frac{1}{p}\frac{dp}{dt}\varepsilon_u\ ,\ \text{where } \tau_u^{-1} = J_u \frac{\overline{P}}{2E},\ \begin{cases} C_x = \overline{\mathcal{H}\frac{\dot{N}<\epsilon^2>}{E^2}} \\ C_y = \frac{\beta_y}{2\gamma^2}\overline{\frac{\dot{N}<\epsilon^2>}{E^2}} \end{cases} \tag{10.29}$$

Longitudinal damping satisfies

$$\frac{d(\widehat{\delta E})^2}{dt} = -\frac{2(\widehat{\delta E})^2}{\tau_l(t)} + (\dot{N}\left\langle\epsilon^2\right\rangle)(t) + \frac{(\widehat{\delta E})^2}{2E}\frac{dE_s}{dt} \quad \text{with } \tau_l^{-1} = J_l \frac{\overline{U_s}}{2E_s} \tag{10.30}$$

******** Figures **??**, **??** display the evolution of horizontal and vertical emittance with time, respectively

Table 10.1 Radiation parameters[(a)], energy loss and equilibrium quantities at the synchronous energy, E_s, in an isomagnetic ring

Critical photon energy, ϵ_c	keV	$\frac{3\hbar\gamma^3 c}{2\rho}$
Average photon energy, $\overline{\epsilon}$	keV	$\frac{8}{15\sqrt{3}}\,\epsilon_c$
rms energy spread, $\sqrt{(\epsilon-\overline{\epsilon})^2}$	keV	$\frac{\sqrt{211}}{15\sqrt{3}}\,\epsilon_c$
Energy loss, U_s	MeV / turn	$C_\gamma \frac{E_s^4}{\rho}$
Nb. of average photons	/turn/particle	$U_s/\overline{\epsilon}$
Longitudinal:		
equil. emittance, $\varepsilon_{l,eq}$	μeV.s	$\frac{\alpha E_s}{\Omega_s}\frac{C_q\gamma^2}{J_l\,\rho}$
rms energy spread, $\sigma_{\delta E/E}$		$\frac{1}{\sqrt{2}}\sigma_{\widehat{\delta E}/E} = \sqrt{\frac{C_q}{J_l\rho}}\gamma$
rms bunch length, σ_l	mm	$\frac{\alpha c}{\Omega_s}\sigma_{\frac{\delta E}{E}}$
Radial:		
equil. emittance, $\varepsilon_{x,eq}$	nm	$= \frac{C_q\gamma^2}{J_x\rho}\bar{\mathcal{H}}$
rms width, $\sigma_x(s)^{(b)}$	m	$\left(\beta_x(s)\varepsilon_{x,eq} + D_x^2(s)\sigma^2_{\frac{\delta E}{E}}\right)^{1/2}$
Damping times, $\tau_{x,y,l}$	ms	$\frac{T_{rev}E_s}{U_s J_{x,y,l}}$

(a) Units are, c: m/s; ρ: m; E_s: GeV
$C_\gamma = \frac{4\pi}{3}\frac{r_0}{(m_0c^2)^3}$ (= $8.846276\,10^{-5}$ m/GeV^3 for electrons).
$C_q = \frac{55}{32\sqrt{3}}\frac{\hbar}{m_0 c}$ (= 3.8319386×10^{-13} m for electrons).
(b) With $\varepsilon_{x,eq}, \beta(s)$ and dispersion $D_x(s)$ in meter.

$$\overline{\epsilon}_{\mathrm{x}}(\mathrm{t}) = \epsilon_{\mathrm{x},0}\left(\mathrm{e}^{\mathrm{t}/|\tau_{\mathrm{x}}|} - 1\right), \qquad \overline{\epsilon}_{\mathrm{y}}(\mathrm{t}) = \epsilon_{\mathrm{y,i}}\,\mathrm{e}^{-\mathrm{t}/\tau_{\mathrm{y}}} \tag{10.31}$$

with $\epsilon_{\mathrm{x},0}$ a constant and $\epsilon_{\mathrm{y,i}}$ an initial value.

10.2.6 Depolarizing resonances

By contrast with weak focusing optics where depolarizing resonances are weak because horizontal field components are weak (Sect. 9.2.3), the use of strong focusing field gradients in the combined function magnets and/or focusing lenses of strong focusing optics results in strong radial field components and therefore strong depolarizing resonances.

Spin precession and resonant spin motion in the magnetic components of a cyclic accelerator have been introduced in Sects. 4.2.5, 5.2.5. The general conditions for depolarizing resonance to occur have been introduced in Sect. 9.2.3. In a strong

focusing synchrotron they essentially result from the radial field components in the focusing magnets and their strength is determined by the lattice optics, as follows.

Strength of imperfection resonances

Imperfection, or integer, depolarizing resonances are driven by a non-vanishing vertical closed orbit $y_{\rm co}(\theta)$ which causes spins to experience periodic radial fields in focusing magnets, dipoles in combined function lattices and quadrupoles in separated function lattices, namely,

$$B_x(\theta) = G\, y(\theta) = K(\theta) \times B_0\rho_0 \times y_{\rm co}(\theta) \tag{10.32}$$

with θ the orbital angle, $B_0\rho_0$ the lattice rigidity and $y_{\rm co}(\theta)$ the closed orbit excursion. Resonance occurs if the spin undergoes an integer number of precessions over a turn (it then undergoes 1-turn-periodic torques), so that spin tilts at field perturbations along the closed orbit add up coherently. Thus resonances occur at integer values

$$G\gamma_n = n$$

A Fourier development of these perturbative fields yields the strength of the $G\gamma_n$ harmonic [23, Sect. 2.3.5.1]

$$\epsilon_n^{\rm imp} = (1+G\gamma)\frac{R}{2\pi}\oint K(\theta)\; y_{\rm co}(\theta)\, e^{-jG\gamma(\theta-\alpha)}\, e^{jn\theta}\, d\theta$$

In the thin-lens approximation, near the resonance where $G\gamma - n \to 0$, this simplifies into a series over the quadrupole fields,

$$\epsilon_n^{\rm imp} = \frac{1+G\gamma_n}{2\pi}\sum_{\rm Qpoles}\left[\cos G\gamma_n\,\alpha_i + \sin G\gamma_n\,\alpha_i\right](KL)_i\; y_{\rm co}(\theta_i) \tag{10.33}$$

with θ_i the quadrupole location, $(KL)_i$ the integrated strength (slice the dipoles as necessary in an AG lattice for this series to converge) and α_i the cumulated orbit deviation.

Orbit harmonics near the betatron tune ($n = G\gamma_n \approx \nu_y$) excite strong resonances. Imperfection resonance strength is further amplified in P-superperiodic rings, with m-cell superperiods, if the betatron tune $\nu_y \approx$ integer $\times\, m \times P$ [24, Chap.3-I].

Strength of intrinsic resonances

Intrinsic depolarizing resonances are driven by betatron motion, which causes spins to experience strong radial field components in quadrupoles, namely

$$B_x(\theta) = G\, y(\theta) = K(\theta) \times B_0\rho_0 \times y_\beta(\theta) \tag{10.34}$$

The effect of resonances on spin depends upon betatron amplitude and phase, their effect on beam polarization depends on beam emittance. Longitudinal fields from dipole ends are usually weak by comparison and ignored. The location of intrinsic resonances depends on betatron tune, it is given in an M-periodic structure by

$$G\gamma_n = nM \pm \nu_y$$

A Fourier development of the perturbative fields yields the two families of strengths [23, Sect. 2.3.5.2]

$$\epsilon_n^{\text{intr}^\pm} = \frac{\lambda_x \rho_0}{4\pi} \int_0^{2\pi} K(\theta) \sqrt{\beta_y(\theta)\frac{\varepsilon_y}{\pi}} e^{\pm j\left(\int_0^{s(\theta)} \frac{ds}{\beta_y} - \nu_y \theta\right)} e^{-jG\gamma(\theta - \alpha(\theta))} e^{jn\theta} d\theta$$

In the thin-lens approximation, near the resonance where $G\gamma \pm \nu_y - n \to 0$, this simplifies into a series over the quadrupole fields,

$$\left\{ \begin{matrix} \mathcal{R}e(\epsilon_n^{\text{intr}^\pm}) + \\ j\ \mathcal{I}m(\epsilon_n^{\text{intr}^\pm}) \end{matrix} \right\} = \frac{1 + G\gamma_n}{4\pi} \sum_{\text{Qpoles}} \left\{ \begin{matrix} \cos(G\gamma_n \alpha_i \pm \varphi_i) + \\ j\ \sin(G\gamma_n \alpha_i \pm \varphi_i) \end{matrix} \right\} (KL)_i \sqrt{\beta_{y,i}\frac{\varepsilon_y}{\pi}} \quad (10.35)$$

10.3 Exercises

In complement to the present exercises, an extensive tutorial on depolarizing resonances in a strong focusing synchrotron, considering proton, helion, or electron beams, using the lattice of the AGS Booster at BNL, can be found in Ref. [23, Chap. 14]. The simulations include the use of tune-jump quadrupoles, a solenoid, Siberian snakes, spin rotators in an electron ring and their effect on polarization life time.

10.1 Construct SATURNE II synchrotron. Spin Dynamics With Snakes

Solution: page 361

Over the years 1978-1997 the 3 GeV synchrotron SATURNE II at Saclay (Fig. 10.8) delivered ion beams up to 1.1 GeV/nucleon, including polarized proton, deuteron and ^{6}Li beams, for intermediate energy nuclear physics research, including meson production [19, 20]. The separated function synchrotron was designed *ab initio* for the acceleration of polarized beams [22], and the first strong focusing synchrotron to do so - ZGS, first to accelerate polarized beams, protons and deuterons, was a weak focusing synchrotron (see Chap. 9).

SATUNE II is a FODO lattice with missing dipole. Its parameters are given in Tab. 10.2.

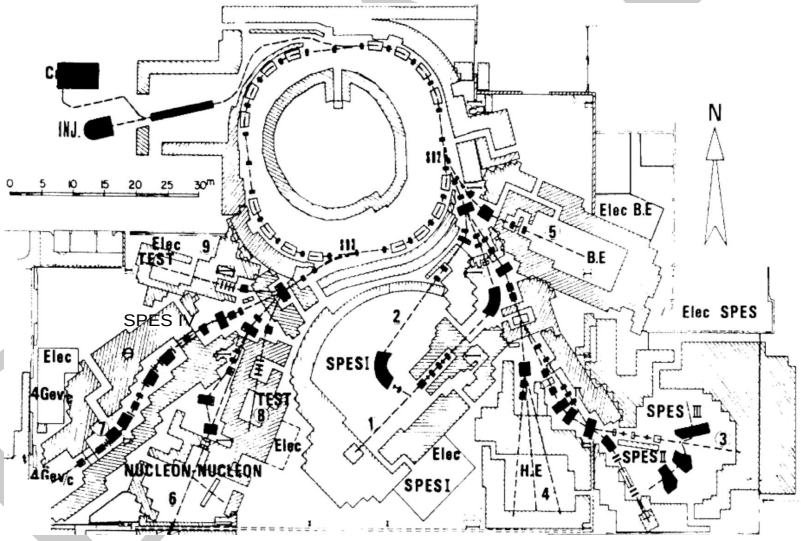

Fig. 10.8 SATURNE II synchrotron and its experimental areas [25], including mass spectrometers SPES I to SPES IV, a typical 1960-80s nuclear physics accelerator facility. Polarized ion sources are on the top left, followed by a 20 MeV linac

(a) Simulate the main dipole using BEND, include fringe fields assuming $\lambda = 8$ cm extent and the following Enge coefficient values (Eq. 15.13, Sect. 15.2.6):

Table 10.2 Parameters of SATURNE II separated function FODO lattice. ρ_0 denotes the reference bending radius in the main dipole; the reference orbit, wave numbers, etc., are taken along that radius

Orbit length, C	m	105.5556
Average radius, $R = C/2\pi$	m	16.8
Length of long straight section	m	
Wave numbers, ν_x; ν_y		3.64; 3.60
Chromaticities, ξ_x; ξ_y		negative, a few units
Momentum compaction α		0.015
Injection energy (proton)	MeV	20
Top energy	GeV	3
$\dot{B}$	T/s	4.2
Synchronous energy gain	keV/turn	1.160
RF harmonic		2
Dipole:		
- bend angle, α	deg	$\pi/8$
- magnetic length, $\rho\alpha$	m	2.489
- magnetic radius, ρ	m	6.3381
- wedge angle, ε	deg	2.45
Quadrupole:		
- gradient	T/m	0.5 - 10.56
- magnetic length F/D	m	0.46723 / 0.486273

$$C_0 = 0.2401,\ C_1 = 1.8639,\ C_2 = -0.5572,\ C_3 = 0.3904,\ C_4 = C_5 = 0$$

Produce a graph of the field across the dipole along the reference orbit, in the median plane and at 5 cm vertical distance. Produce the transport matrix, check against theory. Compare with the matrix of the hard edge model.

Simulate the F and D quadrupoles, using respectively QUADRUPOLE and MULTIPOL. Compare matrices with theory.

Construct the cell. Produce machine parameters (tunes, chromaticities), check against data, Tab. 10.2.

Construct the 4-cell ring. Produce a graph of the optical functions.

(b) Accelerate a bunch with Gaussian densities comprised of a few tens of particles (it can be defined using MCOBJET), from injection to top energy; use harmonic 3 RF frequency, and (unrealistic, for a reduced number of turns) peak RF voltage $\hat{V} = 1$ MV.

Produce a graph of the three phase spaces. Check the transverse betatron damping.

(c) Simulate multiturn injection in the ring. Take the injection point at the center of a long straight section.

(d) Simulate resonant extraction from the ring, on $\nu_x = 11/3$. Take the extraction point at the center of a long straight section.

10.2 Depolarizing Resonances In SATURNE II

The input data file to simulate the ring is given in Tab. 17.73, an outcome of exercise 10.1.

(a) Calculate the strength of the intrinsic depolarizing resonances (systematic and non-systematic) over 0.5-3 GeV, using Eq. 10.35.

(b) Ggamma=7-ν_y was found to be a potentially harmful depolarizing resonance - unexpectedly as this is not a systematic resonance. Produce a crossing of that resonance, for a 100-particle bunch. Get its strength from this simulation, compare with (a).

(c) Multiple resonance xing - ref to Phys. Rev. article ***

10.3 Cornell electron RCS. Radiative Energy Loss

Short intro .... energy loss by synchrotron radiation [26]

Tab.: RCS parameter list

(a) Cornell RCS parameters are given in Tab. **??**. Construct the ring, produce its optical parameters. Produce a graph of the optical functions.

(b) Raytrace a few tens of particles over 3000 turns in Cornell RCS, from *** to *** GeV. Assume emittances epsilx=, epsily=, Gaussian densities, initial *rms* $\delta p/p = 10^{-4}$. Produce a graph of the three phase spaces. produce graphs of horizontal and vertical transverse excursions versus turn number.

(c) Re-do (b) with synchrotron radiation energy loss.

(d) Produce the average beam polarization obtained in (c).

(c) Multiple resonance crossing.

References

1. Christofilos, Nicholas: Focussing system for ions and electrons. US Patent Office Application filed March 10, 1950, Serial No. 148,920. https://patentimages.storage.googleapis.com/fa/bb/52/0ce28e28b492a6/US2736799.pdf
2. Courant, Ernest D., Livingston, M. Stanley, and Snyder, Hartland S.: The Strong-Focusing Synchroton - A New High Energy Accelerator. Phys. Rev. 88, 1190 - December 1952
3. Courant, E.D., and Snyder, H.S.: Theory of the Alternating-Gradient Synchrotron. Annals of Physics, No. 3 (1958), 1âĂŞ48
4. Credit: Brookhaven National Laboratory. https://www.flickr.com/photos/brookhavenlab/8495311598/in/album-72157611796003039/
5. Agapov, I., et al.: Future Circular Lepton Collider FCC-ee: Overview and Status. Submitted on 15 Mar 2022; arXiv:2203.08310 [physics.acc-ph]. https://doi.org/10.48550/arXiv.2203.08310
6. Méot, F., et al.: Progress on the optics modeling of BMIâĂŹs ion rapid-cycling medical synchrotron at BNL. THPMP050, 10th Int. Particle Accelerator Conf. IPAC2019, Melbourne, Australia. https://accelconf.web.cern.ch/ipac2019/papers/thpmp050.pdf Copyrights under license CC-BY-3.0, https://creativecommons.org/licenses/by/3.0; no change to the material
7. Nishimori, N.: A new compact 3 GeV light source in Japan. 13th Int. Particle Acc. Conf. IPAC2022, Bangkok, Thailand. https://accelconf.web.cern.ch/ipac2022/papers/thixsp1.pdf
8. Méot, F.: eRHIC ERL modeling in Zgoubi. BNL-111832-2016-TECH; EIC/49;BNL-111832-2016-IR. https://technotes.bnl.gov/PDF?publicationId=38865
9. Radial Focusing in the Linear Accelerator. Phys. Rev. Vol. 88, Num. 5, Dec. 1, 1952
10. BenabderrahmaneâĂă, C.: Status of the ESRF-EBS magnets. WEPMK009, 9th International Particle Accelerator Conference, IPAC2018, Vancouver, BC, Canada. https://accelconf.web.cern.ch/ipac2018/papers/wepmk009.pdf
11. Credit: Lawrence Berkeley National Laboratory. The Regents of the University of California, Lawrence Berkeley National Laboratory."
12. Jackson, G., Editor: Fermilab recycler ring technical design report. Rev. 1.1. FERMILAB-TM-1981 (July 1996). http://inspirehep.net/record/424541/files/fermilab-tm-1981.PDF
13. Méot, F.: On the Effects of Fringe Fields in the Recycler Ring. FERMILAB-TM-2016 (Aug. 1997). http://inspirehep.net/record/448603/files/fermilab-tm-2016.PDF
14. Ahrens, L., et al.: Development of a stepwise ray-tracing based on-line model at the AGS. WEP141, Proceedings of 2011 Particle Accelerator Conference, New York, NY, USA. https://accelconf.web.cern.ch/PAC2011/papers/wep141.pdf
15. Leleux, G.: Compléments sur la Physique des Accélérateurs. DEA “Physique et Technologie des Grands Instruments”, Université Paris VI. Rapport interne LNS//86-101, CEA Saclay (1986)
16. Leleux, G.: Synchrotron radiation. DEA “Physique et Technologie des Grands Instruments”, Université Paris VI. Rapport interne LNS, CEA Saclay (1991)
17. F. Méot, et al.: Beam dynamics validation of the Halbach Technology FFAG Cell for Cornell-BNL Energy Recovery Linac. Nuclear Inst. and Methods in Physics Research, A 896 (2018) 60âĂŞ67
18. Leleux, G.: Accélérateurs Circulaires. INSTN lectures, internal report CEA Saclay (1978), unpublished
19. The 20 Years of the Synchrotron SATURNE-2. In: Proceedings of the Colloquium, Paris, France, 04 - 05 May 1998, A. Boudard and P.-A. Chamouard Editors. Edited By CEA - Laboratoire National SATURNE & CEN Saclay, France. https://doi.org/10.1142/3965

20. Plus d'anneaux autour de SATURNE (pp. 33-34) Published in: Courrier CERN Volume 39, NÂř 2, Mars 1999.
https://cds.cern.ch/record/1740121
21. Hofmann, A.: The Physics of Synchrotron Radiation. Cambridge Monographs on Particle Physics, Nuclear Physics and Cosmology (20), Cambridge University Press (2004)
22. E. Grorud, J.L. Laclare and G. Leleux: Crossing of Depolarization Resonances in Strongly Modulated Structures. IEEE Transactions on NuclearScience,Vol. NS-26,NO. 3, June 1979.
https://accelconf.web.cern.ch/p79/PDF/PAC1979_3209.PDF
23. Méot, F.: Polarized Beam Dynamics and Instrumentation in Particle Accelerators, USPAS Summer 2021 Spin Class Lectures, Springer Nature, Open Access (2023).
https://link.springer.com/book/10.1007/978-3-031-16715-7
24. Lee, S.Y: Spin Dynamics and Snakes in Synchrotrons. World Scientific (1997)
25. Aknin, J.P., et al.: Status report on rejuvenating SATURNE and future aspects. PAC 1979 Conference. IEEE Tans. Nucl. Sci., Vol. NS 26, No. 3, June 1979.
https://accelconf.web.cern.ch/p79/PDF/PAC1979_3138.PDF
Figure 10.8: Copyrights under license CC-BY-3.0, https://creativecommons.org/licenses/by/3.0; no change to the material; "SPES IV" has been added on the picture
26. D. L. Rubin, et al.: Upgrade of the Cornell electron storage ring as a synchrotron light source. WEPOB36, Proceedings of NAPAC2016, Chicago, IL, USA.
https://accelconf.web.cern.ch/napac2016/papers/wepob36.pdf